J Therm Anal Calorim (2009) 98:47–55
DOI 10.1007/s10973-009-0348-1

# Rapid cooling of lipid in a prilling tower

## Theoretical considerations and consequences on the structure of the microspheres

**Perrine Pivette · Vincent Faivre · Georges Daste · Michel Ollivon · Sylviane Lesieur**

Special Chapter dedicated to the memory of dr. Michel Ollivon


**Abstract** Two lipid binders, glyceryl behenate and paraffin wax, were examined regarding their ability to be used in a prilling process. Prilling has the advantage to produce microgranules very reproducible in size and shape but involves ultrafast cooling of liquid droplets. The different steps to produce solid micropheres from the molten state were successfully modelled to predict crystallisation time as a function of the binder used. Bulk versus microgranules characterization by differential scanning calorimetry, X-ray diffraction and microscopies showed the peculiar suitability of the 50/50 mixture of the two lipid binders for prilling, in agreement with the theoretical approach.

**Keywords** DSC · Glyceryl behenate · Lipid crystallization · Paraffin wax · Prilling · X-ray diffraction

### Introduction

A number of drug candidates notably those synthesized through complex chemical reactions or designed for multiple activities are hydrophobic compounds. The enhancement of their bioavailability can be achieved by their co-administration with lipid-based excipients [1]. For that reason, glycerides and waxes have generated considerable interest for the preparation of oral dosage forms. Solid lipid dispersions offer interesting formulation systems not only for improving apparent solubility of drugs but also for controlling their release rate or even for masking their eventual bitter taste [2–4]. Compared to monolithic forms, divided solid systems for prolonged release present a real advantage in biopharmacy especially in the reproducibility of the stomach filling, then reducing the possibility of physical injury of the digestive tract through the distribution over a large area [5].

Nevertheless, due to polymorphic transitions, lipidic binders can exhibit complex physical state behaviour depending on thermal treatments, time and/or temperature of storage [6–8]. Therefore, to determine their suitability for use in certain pharmaceutical application, it is important to know the thermotropic and structural characteristics of the lipids on both thermodynamic and kinetic levels before evaluating the impact of a specific process on these properties.

The aim of this study is to evaluate the solidification behaviour of lipidic binder mixtures during the production of microgranules by a prilling process. The latter involves heating above melting temperature of the excipients before the extrusion of the molten liquid through calibrated nozzles. Then, by applying a vibration to the nozzles, the jet breaks into calibrated droplets of product which will crystallize by falling into a temperature-controlled atmosphere. In the field of pharmacy, similar methods like spray congealing or melt pelletization have been used to prepare sustained-release formulations [9]. The prilling process has the advantage to produce very well calibrated and smooth microspheres with a narrow size distribution compared to the spraying methods.

Two different lipid binders were investigated in the present study. Paraffin wax (PF) is an inert compound predominantly constituted of straight-chain hydrocarbons

P. Pivette · V. Faivre (✉) · M. Ollivon · S. Lesieur
Université Paris-Sud XI, UMR CNRS 8612, 5 rue J.B. Clément, 92290 Châtenay Malabry, France
e-mail: vincent.faivre@u-psud.fr

G. Daste
Sanofi-Aventis, 20 Avenue Raymond Aron, 92165 Antony, France

($C_nH_{2n+2}$). Compritol® (CP) is a mixture of glyceryl behenates. We focussed on the solid state of both binders separately and in 50/50 (w/w) binary mixture as a function of imposed tempering to anticipate its influence on the stability of further dosage forms and subsequent release. Differential scanning calorimetry (DSC), Small and Wide Angle X-ray Scattering (SAXS–WAXS) and optical and scanning electron microscopies were implemented to understand Compritol® and/or paraffin crystallization behaviours. On one hand, the different steps of the prilling process from the molten liquid to its solidification were modelled by adapting appropriate cooling conditions that could yield the supramolecular arrangement of the microgranules. On the other hand, the structural and thermotropic properties of effectively prilled particles were characterized.

## Experimental

### Materials

Compritol®, a mixture of glyceryl mono-, di- and tri-behenate (18, 52 and 28% by weight, respectively) with a melting temperature range of 69–74 °C, was obtained from Gattefossé (France). Paraffin wax 5205 was purchased from Sasol GmbH (Germany) and has a chain length distribution of a 'normal logarithmic' type ranging from 18 to 45 carbon atoms per chain. The mean and the mode chain length are of 27 and 26 carbon atoms, respectively. The content of iso-alkanes is assessed to about 20% and the melting point at 52–54 °C.

Five gram of a Compritol®/paraffin binary mixture was prepared by mixing 50/50 (wt%) of the two components in a vial and heating the samples on a hotplate around 90 °C. After mixing, the liquid was slowly cooled to room temperature.

### Bulk samples (slow cooling)

In order to avoid effects due to thermal history, all samples were melted around 90 °C, recrystallized at 5 °C $min^{-1}$ and stored 1 week at room temperature before analysis.

### Microgranules (fast cooling)

Pure Compritol®, pure paraffin and the 50/50 (wt%) mixture were melted at 95 °C and extruded through 200-µm nozzles. The vibration technology was used to break the liquid jet in calibrated droplets. The particles were collected after crystallization by falling in a 10 °C temperature-regulated air column. The length of the column was 1.8 m. All samples were stored 1 week at room temperature before analysis.

### Methods

#### *Differential scanning calorimetry*

Differential scanning calorimetry was carried out with a DSC-7 Perkin-Elmer apparatus. Heating and cooling cycles were from 10 to 90 °C with scanning rate of 5 °C $min^{-1}$. To equilibrate the system, 10 min of isotherm was applied between each step. The samples (5 mg average weight) were accurately weighed and sealed in aluminium pans. An empty pan was used as reference and lauric acid (99.5% purity) was used as standard for calibration [10].

#### *X-ray diffraction*

The X-ray diffraction (XRD) experiments were performed on the SAXS beamline (Austrian SAXS beamline, http://www.ibn.oeaw.ac.at/beamline/home.html) of the Elettra synchrotron source (Trieste, Italy). The photon energy was set to 8 keV (radiation wavelength $\lambda$ of 1.549 Å). Data were collected by means of two 1024 channels argon–ethane-filled linear detectors (wide-angle and small-angle acquisition). Cylindrical vacuum chambers equipped with kapton windows were placed in the beam pathway to limit X-ray absorption by air. Wide-angle and small-angle analyses were performed simultaneously by placing the wide-angle detector at a 55° angle from the incident beam direction (sample-to-detector distance of 33 cm) and the small-angle one perpendicular to this direction (sample-to-detector distance of 100 cm). In this configuration, the intervals of scattering vector ($q = 4\pi \sin \theta/\lambda$, where $2\theta$ is the scattering angle) were 0.03–0.54 $Å^{-1}$ and 0.70–1.75 $Å^{-1}$. The repeat distances $d$ characteristic of the structural arrangements were given by $q(Å^{-1}) = 2\pi/d$ (Å). The diffraction patterns were normalized with respect to the acquisition times.

Thin glass capillaries (GLAS, Müller, Berlin, Germany) of 1.5 mm external diameter were used as sample cells. Lipid mixtures (10 mg average weight) were introduced as powders melted around 90 °C and recrystallized at 5 °C $min^{-1}$ 4 days before analysis. Microgranules were directly introduced in the capillary. Silver behenate and tristearin ($\beta$ form) were used as standards to calibrate SAXS and WAXS detector, respectively [11, 12].

#### *Optical microscopy*

Sample preparations were examined by microscopy between crossed polarizers and with a $\lambda/4$ retarder in white light optical using a Nikon E600 Eclipse microscope (Champigny/Marne, France), equipped with a long focus objective (LWD 20 × 0.55; 0–2 mm). The images were recorded with a colour Nikon Coolpix 950 camera at a resolution of 1600 × 1200 pixels. The samples were

placed between two thin circular glass slides (26 mm thick) and observed at different temperatures in the 20–90 °C range and monitored by a hotplate at heating or cooling rates of 5 °C $min^{-1}$.

### *Scanning electron microscopy*

Microgranules were observed by Scanning electron microscopy (SEM) using a Leo 1530 (LEO Electron Microscopy Inc., Thornwood, NY) operating at 3 kV. Samples were coated with palladium platinum layer of about 3 nm, using a Cressington sputter-coater 208HR with a rotary planetary-tilt stage, equipped with a MTM-20 thickness controller.

## Theoretical background

From a thermodynamic point of view, the physical state of a lipid droplet during its fall in the air column evolves according to three main stages: liquid cooling to the melting temperature, crystal growth within the droplet during solidification process, cooling of the solidified droplet. By assuming the pressure as constant, each stage follows specific heat exchange laws which govern the droplet temperature. These can be theoretically predicted as developed below in the approximation that the air injected in the column remains at a constant temperature of 10 °C. Table 1 summarizes the parameters used in the following equations including nomenclature and values from literature data.

### Temperature distribution in the lipid material

The resistance of the heat transfer inside and at the surface of the liquid droplets or solid particles can be appreciated by the calculation of the dimensionless Biot number [19].

The Biot number is defined as:

$$\mathrm{Bi} = \frac{hL_c}{k} \tag{1}$$

where $h$ is the heat transfer coefficient, $k$ is the thermal conductivity of the body of interest and $L_c$ is the characteristic length, commonly described as the volume of the body divided by its surface area.

Strictly, the $L_c$ parameter depends on whether the lipid body is in the molten or the solid state. By assuming the shape of both liquid droplets and solid particles to spheres, their size correlation can be expressed as:

$$d_p = d_d \left(\frac{\rho_m}{\rho_s}\right)^{1/3} \tag{2}$$

**Table 1** List of symbols and values of the physical parameters used in the theoretical approach and subsequent numerical application

| | | |
|---|---|---|
| Bi | Biot number | Dimensionless |
| $C_D$ | Drag coefficient | Dimensionless |
| $\mathrm{Re}_p$ | Single particles Reynolds number | Dimensionless |
| $A$ | Surface of the droplet | $m^2$ |
| $C_{p(m)}$ | Specific heat capacity of molten lipid | [a]kJ $kg^{-1}$ °$C^{-1}$ |
| $C_{p(s)}$ | Specific heat capacity of solid lipid | [a]kJ $kg^{-1}$ °$C^{-1}$ |
| $\Delta H$ | Latent heat of crystallization | kJ $kg^{-1}$ |
| $d_d$ | Diameter of droplet | [b]m |
| $d_p$ | Diameter of particle | [c]m |
| $h$ | Heat transfer coefficient | W $m^{-2}$ °$C^{-1}$ |
| $k$ | Thermal conductivity of lipid | [d]W $m^{-1}$ °$C^{-1}$ |
| $k_a$ | Thermal conductivity of air | [e]W $m^{-1}$ °$C^{-1}$ |
| $L_c$ | Characteristic length | m |
| $m_d$ | Mass of single droplet | kg |
| $\mu_a$ | Viscosity of air | [f]Pa $s^{-1}$ |
| $\rho_a$ | Volumic mass of air | [g]kg $m^{-3}$ |
| $\rho_m$ | Volumic mass of molten lipid | [h]kg $m^{-3}$ |
| $\rho_s$ | Volumic mass of solid lipid | kg $m^{-3}$ |
| $Q$ | Thermal energy | kJ |
| $t_c$ | Time of crystallization | s |
| $T_a$ | Air temperature | [i]°C |
| $T_d$ | Droplet temperature | °C |
| $T_p$ | Particle temperature | °C |
| $U_T$ | Particle terminal velocity | m $s^{-1}$ |

[a] Calculated from heat-flow versus sample amount profiles obtained from calorimetry experiments (data not shown). At 10 °C, $C_{p(s)}$ of Compritol® and paraffin are 1.8 and 1.9 kJ $kg^{-1}$ °$C^{-1}$. $C_{p(m)}$ at 90 °C is 1.9 kJ $kg^{-1}$ °$C^{-1}$ for Compritol® and 2.4 kJ $kg^{-1}$ °$C^{-1}$ for paraffin

[b] Estimated from the particle diameter by considering a ratio of 1.1 between melt lipid and solid lipid volumic mass [12, 13]

[c] The mean microparticle size is 350 µm

[d] A value of 0.17 W $m^{-1}$ °$C^{-1}$ has been used for Compritol® and 0.24 W $m^{-1}$ °$C^{-1}$ for paraffin [14, 15]. Additivity rule has been used for the mixture

[e] At 10 °C, a value of 0.025 W $m^{-1}$ °$C^{-1}$ has been used [16]

[f] A value of $2.0 \times 10^{-5}$ Pa $s^{-1}$ has been used [17]

[g] At 10 °C, a value of 1.225 kg $m^{-3}$ has been used [18]

[h] The volumic mass of molten paraffin was obtained to supplier (775 kg $m^{-3}$ at 70 °C) and that one of Compritol® from supplier and literature (850 kg $m^{-3}$ at 85 °C). Additivity rule has been used for the mixture

[i] Considered as constant (10 °C) in the whole prilling tower

where $d_p$ and $d_d$ are the diameters of particles and droplets, respectively, $\rho_m$ is the volumic mass of the molten lipids and $\rho_s$ the volumic mass of the solid lipids. The ratio $\rho_m/\rho_s$ being estimated to 1.1 for lipidic material [12, 13], the diameter ratio between two types of bodies is very close to 1. The $L_c$ parameter can then be considered as not changed between the liquid and solid states.

Gas to particle heat transfer can be estimated from the following relation given by Kunii and Levenspiel [20]:

$$\frac{hd}{k_a} = 0.03\mathrm{Re}_p^{1.3} \quad (3)$$

where $k_a$ is the thermal conductivity of air and $\mathrm{Re}_p$ is the single particle Reynolds number. Equation 3 is usable as far as $\mathrm{Re}_p$ number is lower than 50. This hypothesis will be checked after calculation.

## Motion of the lipid droplets

Particle Reynolds number could be deduced from drag curves. Indeed, the Reynolds number ranges and drag coefficient ($C_D$) correlations have been described for three regions: the Stokes law region ($\mathrm{Re}_p < 0.3$), the intermediate region ($0.3 < \mathrm{Re}_p < 500$), and the Newton's law region ($500 < \mathrm{Re}_p < 2 \times 10^5$) [21]. In the intermediate region, the correlation is the following one:

$$C_\mathrm{D} = \frac{24}{\mathrm{Re}_\mathrm{p}}\left(1 + 0.15\mathrm{Re}_\mathrm{p}^{0.687}\right) \quad (4)$$

To apply this model, it has been assumed that each droplet is rigid (no deformation) and far from the others or from vessel wall leading to an undistorted flow pattern. Due to the air–lipid interfacial tension, the liquid droplets remain spherical in the air flow and particles are clearly rigid after solidification.

By considering that the particles move with their terminal velocity and that the fluid velocity is negligible compared to that of the particles [22], it is possible to formulate the dimensionless groups, $C_\mathrm{D}\mathrm{Re}_\mathrm{p}^2$ [21]

$$C_\mathrm{D}\mathrm{Re}_\mathrm{p}^2 = \frac{4d^3\rho_\mathrm{a}(\rho_\mathrm{d} - \rho_\mathrm{a})g}{3\quad \mu_\mathrm{a}^2} \quad (5)$$

where $d$ and $\rho_\mathrm{d}$ are the diameter and volumic mass of the droplets (or particles) and $\rho_\mathrm{a}$ and $\mu_\mathrm{a}$ are the volumic mass and viscosity of air.

Equation 6 gives the expression of the single particle terminal velocity, $U_T$:

$$U_\mathrm{T} = \sqrt{\frac{4g(\rho_\mathrm{m} - \rho_\mathrm{a})d_\mathrm{d}}{3C_\mathrm{D}\rho_\mathrm{a}}} \quad (6)$$

## Cooling stages of liquid droplets or completely solidified granules

Considering a homogeneous temperature in the droplets or solid microgranules, it is interesting to predict this temperature and its variation as well as the effective cooling rate of the particles during their fall in the air column.

Among the several models which have been proposed to describe the evolution of the droplet temperature ($T_d$) with time $t$ [23, 24], the most useful is the following one [24, 25]:

$$\frac{\pi d_\mathrm{d}^3}{6}\rho_\mathrm{m}C_{\mathrm{p(m)}}\frac{dT_\mathrm{d}}{dt} = \pi d_\mathrm{d}^2 h(T_\mathrm{a} - T_\mathrm{d}) \quad (7)$$

where $C_{\mathrm{p(m)}}$ is specific heat capacity of the molten lipids and $(T_\mathrm{a} - T_\mathrm{d})$ is the difference of temperature between the droplet and the ambient air.

The previous equation yields the temperature rate profile:

$$\frac{dT_\mathrm{d}}{dt} = \frac{6h(T_\mathrm{a} - T_\mathrm{d})}{\rho_\mathrm{m}C_{p(m)}d_\mathrm{d}} \quad (8)$$

This model can be similarly applied to the cooling process of the solid microparticles by substituting in Eqs. 7 and 8, $d_\mathrm{d}$, $T_\mathrm{d}$, $\rho_\mathrm{m}$ and $C_{\mathrm{p(m)}}$ parameters by $d_\mathrm{p}$, $T_\mathrm{p}$, $\rho_\mathrm{s}$, and $C_{\mathrm{p(s)}}$ ones which correspond to the diameter and temperature of the particles, the volumic mass and specific heat capacity of the lipid in its solid state, respectively.

## Intermediate stage: crystallization of the droplets

In first approximation, time required to achieve crystallisation of one single droplet can be evaluated from DSC measurements. The latent heat of crystallization, $\Delta H$ can be deduced from the area under the DSC crystallization peak that gives the heat energy exchange for a given sample mass $Q$. For a single droplet:

$$\Delta H = \frac{Q}{m_\mathrm{d}} \quad (9)$$

where $m_\mathrm{d}$ is the mass of a single droplet.

Besides, by assuming that the crystallization process is an isothermal transition, the heat lost Q provoked by the liquid-to-solid transition is given by the heat transfer coefficient of the lipids as follows:

$$m_\mathrm{d}\Delta H = hA(T_\mathrm{d} - T_\mathrm{a})t_\mathrm{c} \quad (10)$$

where $A$ is the surface of the droplet, $(T_\mathrm{d} - T_\mathrm{a})$ the difference of temperature between the droplet and the ambient air and $t_\mathrm{c}$ the crystallization duration. Here the $T_\mathrm{d}$ value is considered as constant and equal to the onset crystallization temperature $T_\mathrm{c}$. By approximating that the droplet is liquid until the end of the crystallization and the liquid and solid states have the same volumic mass ($\rho_\mathrm{m} \sim \rho_\mathrm{s}$), duration of crystallization achievement can be deduced from Eqs. 9 and 10 as follows:

$$t_c = \frac{\Delta H \rho_m L_c}{h(T_c - T_a)} \quad (11)$$

## Results and discussion

### Phase behaviour of Compritol®, paraffin and 50/50 (w/w) mixture: comparison of the bulk state and microgranules

Figure 1 shows XRD patterns of paraffin, glyceryl behenate and their 50/50 (w/w) mixture recorded at 20 °C either as bulk matrices or constituting microgranules. Table 2 summarizes the long- and short-range distances characteristic of the different lipid packings. Paraffin wax exhibits wide-angle Bragg reflections at 4.2 Å ($q = 1.50$ Å$^{-1}$) and 3.7 Å ($q = 1.68$ Å$^{-1}$) characteristic of the expected orthorhombic subcell organization of the hydrocarbon chains [26, 27]. The small-angle diffraction pattern reveals the first and second order-peaks of a 2L lamellar structure with a repeat distances of 37.3 Å in the bulk and 37.3 Å for the microgranules. The structural behaviour of complex n-alkanes mixtures mainly depends on the chain length distribution law [28, 29]. While exponentially decreasing distributions lead to the formation of multiple solid solutions, log-normal distributions are generally compatible with the existence of unique solid solutions. The co-packing of hydrocarbon chains with dissimilar lengths is compensated by longitudinal molecular shifts [30, 31]. The periodicity of the molecular layer stacking in a multi-alkane solid solution is equal to the average length of the chains in the mixture with an excess value usually of 1–2 carbon atoms [29]. In the present study, the measured lamellar repeat distances of the occurring solid solution are equivalent to chain length of 28 carbon atoms, according to n-alkane crystallographic data [32]. That is consistent with the PF studied which presents an average chain size centred on 26 carbon atoms. Acyl glycerols are characterized by a complex polymorphic behaviour, often linked to the existence of monotropic transitions. The phases formed in the solid state and their molecular structures highly depend on thermal history, cooling rate, sample size and composition [7, 33, 34]. Compritol® SAXS patterns at 20 °C mainly show a 2L lamellar packing with repeat distances slightly varying from 61.6 Å for lipids in the bulk sample to 62.4 Å in the case of the microgranules (Fig. 1). This variation of the lamellar periodicity is accompanied by a perceptible broadening of the Bragg reflections and might be due to a hindering of organization of the acyl glycerol molecules in the solid state during the formation of microgranules. This indeed could modify layer stacking and generate structural defects and/or reduce the size of crystal units. With respect to the short-range distance, WAXS recording shows that the hydrocarbon chains arrange in a pseudohexagonal subcell called *Sub* α as already described [35]. As a whole, the individual crystalline structures of Compritol® and paraffin are mainly preserved in the binary mixture and no new structure appears. The Bragg reflections occur almost at the same positions whether the sample is aliquot of bulk matrix or microsphere preparation. However, the diffraction peaks related to Compritol® contribution within the microspheres appear broader and less intense than those characterizing the slowly cooled binary mixture in bulk. Nevertheless, the voids in the sample due to inter-particle space being able to be around 30% for spherical particles, the lowering of peak intensity could be partly due to the consequent decrease in effective optical pathway through lipid material.

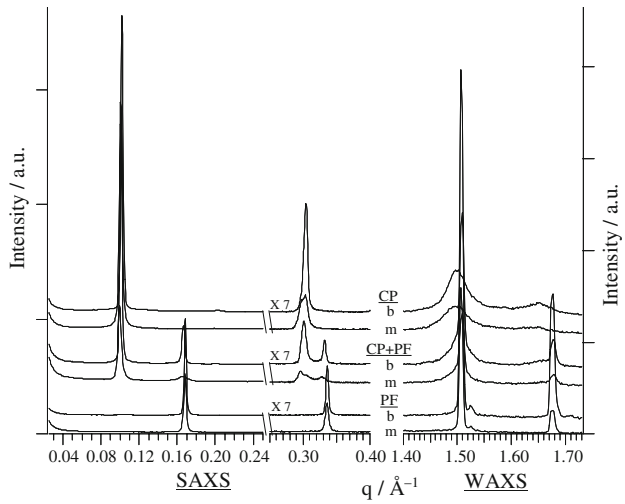


**Fig. 1** SAXS/WAXS profiles at 20 °C of Compritol® (CP), paraffin (PF) and Compritol®/paraffin binary mixture (50/50 w/w) (CP + PF) in the bulk state (*b*) (slowly crystallized at 5 °C min$^{-1}$) and in the microgranules (*m*) (fast cooling by prilling process). Intensity was increased by a factor 7 to emphasize diffraction lines of upper orders in the 0.24–0.40 Å$^{-1}$ q range

**Table 2** Structural parameters of Compritol® (CP), paraffin (PF) and Compritol®/paraffin binary mixture (50/50 w/w) (CP + PF) in the bulk state (*b*) (slowly crystallized at 5 °C min$^{-1}$) or in the microgranules (*m*) (fast cooling by prilling process) from Small- and Wide-Angle X-ray diffraction (SAXS/WAXS) profiles at 20 °C

| Sample | | *d*/Å | | | |
|---|---|---|---|---|---|
| | | SAXS | | WAXS | |
| CP | *b* | 61.6 | | 4.2 | 3.8 |
| | *m* | 62.4 | | 4.2 | 3.8 |
| CP + PF | *b* | 62.3 | 37.7 | 4.2 | 3.7 |
| | *m* | 63.2 | 37.9 | 4.2 | 3.7 |
| PF | *b* | | 37.3 | 4.2 | 3.7 |
| | *m* | | 37.3 | 4.2 | 3.7 |

To investigate the thermotropic behaviour of the binders as a function of their microscopic dispersion state, DSC analyses of the same Compritol® and/or paraffin samples as those analyzed by XRD were carried out at a rate of 5 °C $min^{-1}$. In the case of lipids in bulk, successive cooling and heating scans were recorded in the 10–90 °C range while in the case of microgranules, only one heating scan from 10 to 90 °C was performed to conserve the microstructure produced by the prilling process. The resulting curves are shown in Fig. 2A and B. Table 3 gathers the melting parameters, i.e., the onset melting temperatures $T_{onset}$ and fusion enthalpy variations $\Delta H$ deduced from the surface areas of the endothermic events.

For both separate components, solid–solid transitions are observed at low temperature: $T_{onset}$ of 26 °C for the orthorhombic to hexagonal chain packing transition of paraffin [36–39] and $T_{onset}$ of 20 °C for the pseudohexagonal to hexagonal chain packing transition of Compritol® [35]. These two transitions are reversible. Then paraffin melts at 47.5 °C and Compritol® at 70 °C.

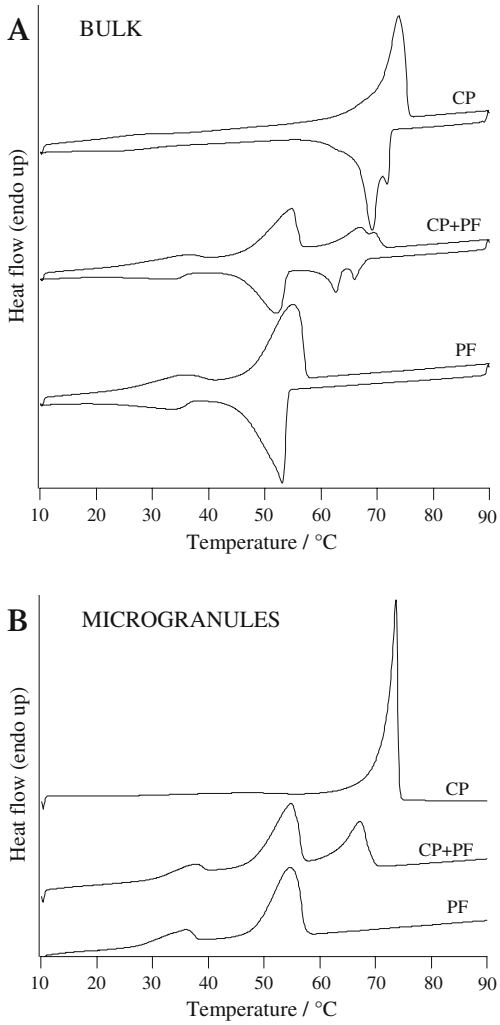


**Fig. 2** Differential scanning calorimetry (DSC) curves of Compritol® (CP), paraffin (PF) and Compritol®/paraffin binary mixture (50/50 w/w) (CP + PF) in the bulk state (**A**) and in the microgranules (**B**); scans were performed at 5 °C $min^{-1}$

When mixed in bulk, glyceryl behenates and paraffinic alkanes show separate exothermic crystallization events and melting endotherms which occurred in temperature ranges close to those observed for the individual components. This confirms the supramolecular segregation of the two binders in the solid state as observed by XRD. Melting behaviour of the lipids forming microgranules did not reveal significant differences compared to those in the bulk state. As it is mentioned in Table 3, Compritol® melting transition enthalpy in the binary mixture did not correspond to 50% of the melting transition enthalpy of the pure CP sample. The two binders seem then partially miscible.

Polarized light microscopy of the Compritol® and paraffin binary mixture was performed from 90 down to 20 °C (Fig. 3). At 80 °C, an isotropic liquid is observed. Then, in agreement with DSC, the first crystallites presumably rich in Compritol® appear at around 70 °C. The distribution of the crystals within liquid paraffin is homogeneous without segregation of the observed sample. Finally, a second population of crystals, certainly paraffin, appears around 50 °C. Hot stage microscopy with polarized light on binary mixtures confirms melting and crystallisation temperature. Furthermore, it shows the absence of any long-range segregation. This is an important point to take into account for the preparation of homogeneous microspheres with these two binders.

## Numerical applications

The main results given by the numerical applications of equations developed in the theoretical section are reported by Table 4. From data in Table 1 and the set of Eqs. 4 and 5 estimate values of $Re_p$ and $C_D$ are obtained for Compritol®, Paraffin and their mixture and are found below 50 so that Eq. 4 is indeed relevant for the systems studied. Then, particle to gas heat transfer coefficients, $h$, can be calculated from Eq. 3 and are found in the 137–151 W $m^{-2}$ $K^{-1}$ range, depending on the compound of interest.

The *Biot* numbers deduced from Eq. 1 are smaller than 0.1. This implies that the heat conduction inside the body is much faster than the heat conduction away from the surface and that temperature gradients within the droplets are negligible [19, 25]. This means that, upon cooling in the air column, the temperature inside the liquid droplets at the beginning of the process and then inside the solid granules throughout their fall in the tower, can be considered as homogenous. By applying Eqs. 7 and 8, the modulus of cooling rate could then be calculated and expressed as a function of the instantaneous droplet temperature (Fig. 4). It is worth noting that the cooling rates are very fast,

**Table 3** Melting transition temperatures and enthalpies of Compritol® (CP), paraffin (PF) and Compritol®/paraffin binary mixture (50/50 w/w) (CP + PF) in the bulk state (slowly crystallized at 5 °C $min^{-1}$) and in the microgranules (fast cooling by prilling process). For the mixture, enthalpies are expressed per g of total material

| Melting transitions | | | | | | | | |
|---|---|---|---|---|---|---|---|---|
| Sample | Bulk | | | | Microgranules | | | |
| | $PF_{melt}$ | | $CP_{melt}$ | | $PF_{melt}$ | | $CP_{melt}$ | |
| | $T_{onset}$/°C | $\Delta H$/J $g^{-1}$ | $T_{onset}$/°C | $\Delta H$/J $g^{-1}$ | $T_{onset}$/°C | $\Delta H$/J $g^{-1}$ | $T_{onset}$/°C | $\Delta H$/J $g^{-1}$) |
| CP | | | 70.1 | 128.6 | | | 71.7 | 126.1 |
| CP + PF | 46.9 | 69.0[a] | 61.8 | 37.8[a] | 48.2 | 69.2 | 62.3 | 44.2 |
| PF | 47.5 | 138.1 | | | 48.2 | 145.0 | | |

[a] By assuming additivity rule of the transition enthalpies, the theoretical melting transition enthalpies of paraffin and Compritol® in the mixture would be 69.1 and 64.3 J $g^{-1}$, respectively

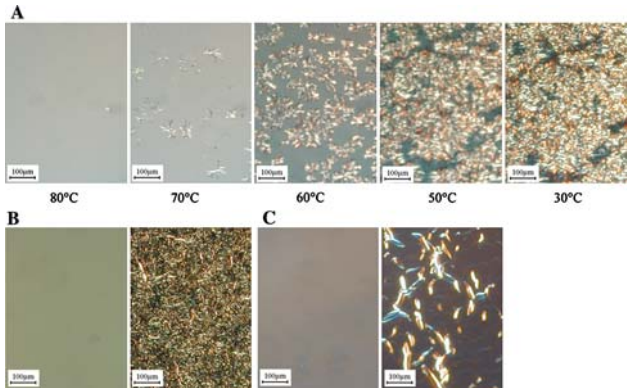


**Fig. 3** **A** Compritol®/paraffin binary mixture (50/50 w/w), crystallisation from 80 to 30 °C at 5 °C $min^{-1}$; **B** Compritol®, crystallisation from 80 to 70 °C at 5 °C $min^{-1}$; **C** paraffin, crystallisation from 60 to 50 °C at 5 °C $min^{-1}$; observed with polarized light microscopy

**Table 4** Summary of the numerical applications for Compritol® (CP), paraffin (PF) and the binary mixture (CP/PF)

| | CP | CP/PF | PF |
|---|---|---|---|
| Bi | 0.05 | 0.04 | 0.03 |
| $C_D$ | 2.2 | 2.2 | 2.3 |
| $Re_p$ | 27 | 26 | 25 |
| $h$/W $m^{-2}$ $K^{-1}$ | 151 | 144 | 137 |
| $U_T$/m $s^{-1}$ | 1.2 | 1.2 | 1.1 |
| $t_c$/s | 0.7 | 0.4[a] | 1.0 |

[a] By assuming additivity rule of the transition enthalpies, the crystallization time would be 0.9 s

thousands of °C $min^{-1}$ in the "droplet cooling region", for the three investigated systems. The calculations give particle terminal velocities, $U_T$ values, around 1.1–1.2 m $s^{-1}$ that is about 10 times faster than the velocity of the co-axial air stream in the prilling tower, indeed slower than 0.1 m $s^{-1}$. This verifies that Eq. 5 is relevant for describing the system studied here. By using $\Delta H$ and $T_c$ values from

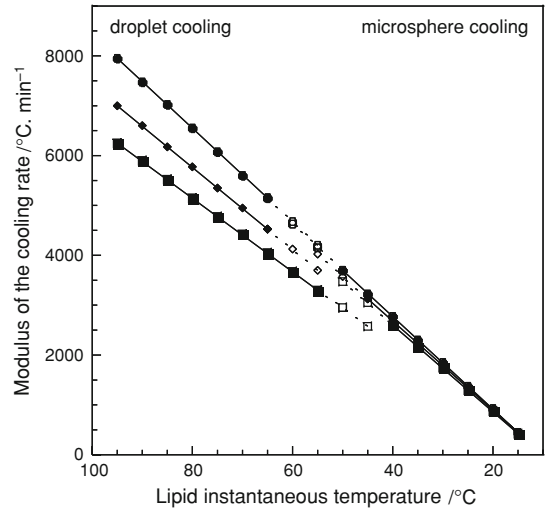


**Fig. 4** Modulus of the cooling rates of the droplets and microspheres as a function of their temperature during their fall in the air column: (*filled circle*) Compritol®, (*filled square*) paraffin, (*filled diamond*) 50/50 binary mixture. *Dashed lines* and *open symbols* correspond to crystallization regions in which the model equations are not usable

Table 3, it is possible to calculate single particle crystallization times from 0.4 to 1 s. The latent heats of melting have been used in the calculations as they are similar to latent heats of crystallization (comparison not shown), but their determinations are more precise because of the curve profiles. Compared to pure compounds, the 50/50 binary mixture appears to more easily crystallize as the latent heat of the solid-to-liquid transition is decreased for the Compritol® rich fraction.

Indeed, the binary mixture crystallization time obtained from the experimental values reaches 0.4 s while it would be around 0.9 s by considering a strict physical mixture without any intercomponent miscibility.

From the cooling rate profiles in Fig. 4, it is possible to predict the time required for a droplet to reach crystallization temperature. Taking into account the additive time required for achieving crystallization, an estimate of the

minimum fall time necessary to obtain solid microgranules is then around 0.9, 1.5 and 0.9 s for Compritol®, paraffin and their 50/50 mixture. Compared to the fall durations of the particles in the device used for prilling and evaluated to 1.5, 1.6 and 1.5 s, respectively, it appears that solid microgranules must have been yielded in the experimental conditions used. However, one additive factor was not considered in the theoretical approach. That is the rate of nucleation and associated supercooling behaviour of the lipid binders, indeed shown by DSC cooling scans recorded for the lipids in the bulk state at a moderate tempering rate. This phenomenon might significantly shift the time necessary to achieve crystallization within the prills all the more so as crystallization within dispersed liquid structures is known to be less easy than in continuous systems.

From the previous results, the paraffin alone behaves closely to the limits of the process as it is apparent by comparing the minimum fall time necessary to obtain solid microgranules with the fall time duration. The fall duration is certainly underestimated because the terminal velocity used for the calculations corresponds to a constant velocity which is the maximum attainable. The instantaneous velocity at any time during the fall depends on the acceleration of the droplet, produced in response to Newton's first law of motion, and the balance of forces acting on it. Due to gravitation, this velocity increases with time and becomes constant when the drag becomes equal to the weight, leading to vertical acceleration equal to zero. The droplets being very small and the motion fast, it was not possible to measure experimentally the real fall duration in the prilling tower. Moreover, if the fall duration is enough and the crystallization achieved, the recovered prills should appear spheroidal in shape since solid state impedes any surface deformation when the particles strike the bottom of the tower. SEM images seen in Fig. 5 reveal perfect sphericity of the particles, even with paraffin, which definitely show that complete crystallization has time to occur during the fall duration. No traces of impaction are visible on the microgranule surfaces, confirming their crystallization before reaching the prilling device walls.

The XRD results showed that bulk samples submitted to slow cooling arrange in the same structure as that observed for microspheres formed upon fast cooling. However, it is worth noting that in thermal conditions leading to the melting of part or totality of the lipids constituting dispersed systems, structural modification can occur [8, 40]. Indeed, upon ageing of the microspheres at room temperature, a slight improvement of the WAXS peak resolution could be observed in the case of CP (data not shown). As such a behaviour may influence the release kinetics of drugs loaded within the particles [41], structural evolution deserves special attention and must be very carefully investigated. In this respect, further work concerning drug-loaded microspheres is now in progress.

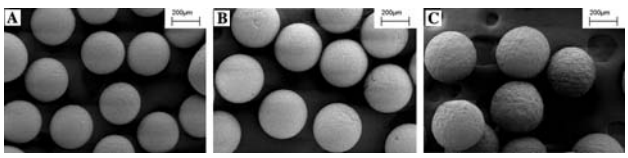


**Fig. 5** SEM images of microgranules obtained by prilling process and based on **A** Compritol®, **B** Compritol®/paraffin (50/50 w/w), **C** paraffin

## Conclusions

The combination of thermal analysis by DSC with structural characterization at the molecular scale by XRD at both small and wide angles and at the supramolecular one by microscopy allowed to characterize the ability of two lipid binders based either on alkanes or behenate glycerides to form calibrated solid microparticles by prilling process. Mainly, the results here give the evidence that the 50/50 (w/w) binary mixture of paraffin and Compritol® form an alloy-like solid state although individual structural organization and thermal properties are globally preserved. Despite of a fast cooling during the fall in the air column and supercooling risk, prilling process does not seem to strongly affect this solid state as it was predicted by theoretical approach and proven by investigations on the final structure of microspheres. In this case, the fast cooling rate leads to the same crystalline structure for Compritol®, paraffin or Compritol®/paraffin mixture. Even if lipid excipients have a complex polymorphism, regarding the cooling rate we show here that Compritol® and paraffin could be well-adapted for a prilling application.

This behaviour depends on binders interactions. It is clear from this study that the transition enthalpies related to the mixture of CP and paraffin are not proportional to the respective amounts, suggesting interactions (intersolubility) between the two binders. Because lipid organization containing guest molecules are susceptible to re-arrange, these interactions between Compritol® and paraffin will be deeply investigated in another study.

Nucleation and crystallization kinetics depending on the compound of interest, it should be very interesting to measure these rates with the present and other binders. Various measurement techniques have been employed to quantify nucleation rates such as DSC, turbidimetry or polarized light microscopy [34]. However, to be powerful in our study and to take into account probabilistic distribution of the nuclei in the binder droplets, the difficulty will be to keep the dispersed state of the prills even in the melt state.

**Acknowledgements** The authors wish to express their thanks to Heinz Amenitsch from the ELETTRA synchrotron (Trieste, Italy), Nicolas Tsapis for his help in the SEM observations and Audrey Allavena-Valette (CECM, Vitry sur Seine) for access to the SEM facility.

## References

1. Porter CJH, Trevaskis NL, Charman WN. Lipids and lipid-based formulations: optimizing the oral delivery of lipophilic drugs. Nat Rev Drug Discov. 2007;6:231–48.
2. Hauss DJ. Oral lipid-based formulations. Adv Drug Deliv Rev. 2007;59:667–76.
3. Guse C, Koennings S, Kreye F, Siepmann F, Goepferich A, Siepmann J. Drug release from lipid-based implants: elucidation of the underlying mass transport mechanisms. Int J Pharm. 2006;314:137–44.
4. Hamdani J, Moës AJ, Amighi K. Development and evaluation of prolonged release pellets obtained by the melt pelletization process. Int J Pharm. 2002;245:167–77.
5. Bechgaard H, Brodie RR, Chasseaud LF, Houmøller P, Hunter JO, Siklos P, et al. Bioavailability of indomethacin from two multiple-units controlled-release formulations. Eur J Clin Pharmacol. 1982;21:511–5.
6. Sutananta W, Craig DQM, Newton JM. An investigation into the effect of preparation conditions on the structure and mechanical properties of pharmaceutical glyceride bases. Int J Pharm. 1994;110:75–91.
7. Sato K. Crystallization behaviour of fats and lipids—a review. Chem Eng Sci. 2001;56:2255–65.
8. Hamdani J, Moës AJ, Amighi K. Physical and thermal characterisation of Precirol® and Compritol® as lipophilic glycerides used for the preparation of controlled-release matrix pellets. Int J Pharm. 2003;260:47–57.
9. Jannin V, Musakhanian J, Marchaud D. Approaches for the development of solid and semi-solid lipid-based formulations. Adv Drug Deliv Rev. 2008;60:734–46.
10. Grabielle-Madelmont C, Perron R. Calorimetric studies on phospholipid-water systems, I. DL-dipalmitoylphosphatidylcholine (DPPC)-water system. J Colloid Interface Sci. 1983;95:471–82.
11. Huang TC, Toraya H, Blanton TN, Wu Y. X-ray powder diffraction analysis of silver behenate, a possible low-angle diffraction standard. J Appl Cryst. 1993;26:180–4.
12. Ollivon M, Perron R. Propriétes physiques des corps gras. In: Karleskind A, Wolff JP, editors. Manuel des corps gras. Paris: Lavoisier; 1992.
13. Gunstone FD, Harwood JL, Padley FB. The lipid handbook. London: Chapman & Hall; 1986.
14. Bugaje IM. Enhancing the thermal response of latent heat storage systems. Int J Energy Res. 1997;21:759–66.
15. Tavman IH, Tavman S. Measurement of thermal conductivity of dairy products. J Food Eng. 1999;41:109–14.
16. Kreith F. CRC handbook of thermal engineering. Boca Raton: CRC Press; 2000.
17. Wu Y, Bao C, Zhou Y. An innovated tower-fluidized bed prilling process. Chin J Chem Eng. 2007;15:424–8.
18. Weast RC. CRC handbook of chemistry and physics. 70th ed. Boca Raton: CRC Press; 1990.
19. Crowe C, Sommerfeld M, Tsuji Y. Multiphase flows with droplets and particles. New York: CRC Press; 1998.
20. Kunii D, Levenspiel O. Fluidization engineering. 2nd ed. Chichester: Wiley; 1990.
21. Rhodes M. Introduction to particle technology. 2nd ed. Chichester: Wiley; 2008.
22. Limousin V. Le prilling, procédé de choix pour les formes solides. Informations Chimie. 1997;389:124–7.
23. Bakhatin LA, Vagin AA, Esipovich LY, Labutin AN. Investigation and calculation of thermochemical process: heat-exchange calculations in prilling towers. Khimicheskoe i Neftyanoe Mashinostroenie. 1978;11:13–6.
24. Laurent S, Puiggali JR, Roques M. Elements de dimensionnement d'une technique d'égouttage en vue d'une extrapolation industrielle. Entropie. 1997;204:11–9.
25. Gwie C, Griffiths R, Cooney D, Johns M, Wilson D. Microstructures formed by spray freezing of food fats. J Am Oil Chem Soc. 2006;83:1053–62.
26. Dorset DL. Role of symmetry in the formation of n-paraffin solutions. Macromolecules 1987;20:2782–8.
27. Small DM. Lateral chain packing in lipids and membranes. J Lipid Res. 1984;25:1490.
28. Briard A-J, Bouroukba M, Petitjean D, Hubert N, Moïse J-C, Dirand M. Thermodynamic and structural analyses of the solid phases in multi-alkane mixtures similar to petroleum cuts at ambient temperature. Fuel. 2005;84:1066–73.
29. Dirand M, Chevallier V, Provost E, Bouroukba M, Petitjean D. Multicomponent paraffin waxes and petroleum solid deposits: structural and thermodynamic state. Fuel. 1998;77:1253–60.
30. Chevallier V, Provost E, Bourdet JB, Bouroukba M, Petitjean D, Dirand M. Mixtures of numerous different n-alkanes: 1. Structural studies by X-ray diffraction at room temperature—correlation between the crystallographic long c parameter and the average composition of multi-alkane phases. Polymer. 1999; 40:2121–8.
31. Petitjean D, Schmitt JF, Laine V, Bouroukba M, Cunat C, Dirand M. Presence of isoalkanes in waxes and their influence on their physical properties. Energy & Fuels. 2008;22:697–701.
32. Nyburg SC, Potworowski JA. Prediction of units cells and atomic coordinates for the n-alkanes. Acta Cryst. 1973;B29:347–52.
33. Small DM. The physical chemistry of lipids. In: Hanahan DJ, editors. Handbook of lipid research. New York: Plenum Press; 1986.
34. Himawan C, Starov VM, Stapley AGF. Thermodynamic and kinetic aspects of fat crystallization. Adv Colloid Interface Sci. 2006;122:3–33.
35. Brubach JB, Jannin V, Mahler B, Bourgaux C, Lessieur P, Roy P, et al. Structural and thermal characterization of glyceryl behenate by X-ray diffraction coupled to differential calorimetry and infrared spectroscopy. Int J Pharm. 2007;336:248–56.
36. Chazhengina SY, Kotelnikova EN, Filippova IV, Filatov SK. Phase transitions of n-alkanes as rotator crystals. J Mol Struct. 2003;647:243–57.
37. Chevallier V, Petitjean D, Bouroukba M, Dirand M. Mixtures of numerous different n-alkanes: 2. Studies by X-ray diffraction and differential thermal analyses with increasing temperature. Polymer. 1999;40:2129–37.
38. Dirand M, Bouroukba M, Briard A-J, Chevallier V, Petitjean D, Corriou J-P. Temperatures and enthalpies of (solid + solid) and (solid + liquid) transitions of n-alkanes. J Chem Thermodyn. 2002;34:1255–77.
39. Nowak MJ, Severtson SJ. Dynamic mechanical spectroscopy of plastic crystalline states in n-alkane systems. J Mater Sci. 2001; 36:4159–66.
40. Reitz C, Kleinebudde P. Influence of thermal and thermomechanical treatment. J Therm Anal Calorim. 2007;89:669–73.
41. Choy YW, Khan N, Yuen KH. Significance of lipid matrix aging on in vitro release and in vivo bioavailability. Int J Pharm. 2005;299:55–64.